

# Prognostics and Health Management of an Electro-Hydraulic Servo Actuator

Andrea Mornacchi<sup>1</sup>, George Vachtsevanos<sup>2</sup> and Giovanni Jacazio<sup>3</sup>

<sup>1,3</sup> *Politecnico di Torino - Department of Mechanical and Aerospace Engineering, Turin, 10129, Italy*

*andrea.mornacchi@polito.it*  
*giovanni.jacazio@polito.it*

<sup>2</sup> *Georgia Institute of Technology, Atlanta, GA, 30332, USA*

*giv@ece.gatech.edu*

## ABSTRACT

Electro-Hydraulic Servo Actuators (EHSA) is the principal technology used for primary flight control in new aircrafts and legacy platforms. The development of Prognostic and Health Management technologies and their application to EHSA systems is of great interest in both the aerospace industry and the air fleet operators.

This paper presents the results of an ongoing research activity focused on the development of a PHM system for fly-by-wire primary flight EHSA. One of the key features of the research is the implementation of a PHM system without the addition of new sensors, taking advantage of sensing and information already available. This choice allows extending the PHM capability to the EHSAs of legacy platforms and not only to new aircrafts. The enabling technologies borrow from the area of Bayesian estimation theory and specifically particle filtering and the information acquired from EHSA during pre-flight check is processed by appropriate algorithms in order to obtain relevant features, detect the degradation and estimate the Remaining Useful Life (RUL). The results are evaluated through appropriate metrics in order to assess the performance and effectiveness of the implemented PHM system.

## 1. INTRODUCTION

Flight control systems and their associated flight control servoactuators are one of the critical aircraft systems and belong to the top operational disruption contributors. Developing effective PHM algorithms for primary flight control actuators that can be integrated in a health monitoring system for the entire aircraft flight control

system will lead to a valuable technological advancement.

The benefits achievable from developing an efficient health monitoring system able to anticipate the failures of the aircraft flight control system fall in two areas:

- Improvement of the aircraft operational reliability and dispatchability by avoiding:
  - Aircraft on ground immobilization
  - Takeoff delays and cancellations
  - Re-routing
  - In-flight turn back
- Reduction of direct maintenance costs by:
  - Performing maintenance operations of anticipated failures at an airline main base
  - Improving troubleshooting of failures
  - Reducing scheduled maintenance operations and rescheduling some recurring maintenance tasks

Costs related to unscheduled maintenance operation and to flight disruptions resulting from unexpected failures may vary in a relatively large range, depending on the type of aircraft and of its flight control system, on the operational environment, on the maintenance policies and on the aircraft usage. Though not easily quantifiable, these costs are at present a large fraction of the life cycle cost.

- Assuming an average cost related to unexpected failures equal to 30% of the system total life cycle cost, which is a conservative underestimate, the development of a health management system for the aircraft flight controls able to reduce to half that cost would provide a tremendous benefit to the aircraft operation.
- It is also generally accepted that the average cost for an aircraft downtime is equal to about US\$ 10000 per

Andrea Mornacchi et al. This is an open-access article distributed under the terms of the Creative Commons Attribution 3.0 United States License, which permits unrestricted use, distribution, and reproduction in any medium, provided the original author and source are credited.

hour (Pohl, 2013), therefore, also a minor reduction of the average aircraft downtime for an aircraft fleet entails very large savings.

IATA projection for global spending in 2020 for maintenance, repair and overhaul is US\$ 65 billion (IATA, 2011). Although the spending for flight control actuators will be only a fraction of that total figure, it is evident that the contribution gained from the introduction of an effective health monitoring system for aircraft flight control actuators will still contribute to a large cost saving for maintenance operations. Another large cost saving is obtained from the reduction of flight disruptions and delays. A recent study on integrated disruption management and flight planning shows that suitable planning can mitigate the effects of flight disruptions and lead to about 6% cost saving for the airline (Marla, Vaaben, Barnhart, 2011). Though this study did not specifically refer to health monitoring systems, it provides an indication of the order of magnitude of the cost savings that can be attained by reducing flight disruptions and delays.

It is therefore easy to understand how the Prognostic and Health Management (PHM) systems has found an intense interest in the aerospace area over the past years. Primary flight control systems are an engineering area where PHM has found so far very limited interest, although they are one of the critical aircraft systems. Some work has been reported on PHM for electromechanical flight control actuators, but almost very little or nothing for electrohydraulic servo-actuators (EHSAs) for primary flight controls. However, although electromechanical actuators (EMA) for primary flight control systems are long-term objectives, sensitivity to certain single point of failures that can lead to mechanical jams, results in a reluctance to adopt EMAs for flight safety critical applications. EMAs for primary flight controls have so far been limited to UAVs (Jacazio, 2008). It should be pointed out that primary flight control actuators for fly-by-wire commercial aircraft in service and for aircraft under development are almost invariably electrohydraulic servo-actuators; the only exception are some electro-hydrostatic actuators (EHA) used as a backup to conventional EHSAs in the flight control systems of Airbus A380, A350 and Gulfstream G650. "Electro-hydraulic servovalves (EHSVs) are a critical component of EHSAs, they are made up by a large number of parts and can thus fail as a result of several causes. The research work presented in this paper was therefore focused on developing a PHM system able to identify the progressive degradations of EHSVs and alert of a developing failure. The research activity will then continue addressing the faults of the hydraulic linear actuator"

Research and development of PHM systems for primary flight controls focused mostly on EMAs due to the growing interest in Unmanned Aerial Vehicle (UAV); moreover, the EMAs have a greater probability of critical failure than

EHSAs. Byington, Watson and Edwards (2004) presented one of the few research papers focused on the hydraulic actuators for aviation. The authors examine the possibility of developing a PHM system for the F/A-18 stabilizer Electro-Hydraulic Servo-Valves (EHSVs). The data-drive approach developed uses neural network error-tracking techniques, along with fuzzy logic classifiers, Kalman filter state predictors, and feature fusion strategies. An interesting work was presented by NASA Ames Research Center (Narasimhan, Roychoudhury, Balaban & Saxena, 2010). The paper proposed a combined model-based and feature-driven diagnosis methodology that allows the detection of the common EMAs fault modes. Brown et al. (2009a and 2009b) have shown the possibility of exploiting the particle filter for the diagnostics and prognostics of EHAS.

The major objective of this contribution is to develop an innovative fault diagnosis and failure prognosis framework for critical aircraft components that integrates effectively and mathematically rigorous and validated signal processing, feature extraction, diagnostic and prognostic algorithms with novel uncertainty representation and management tools in a platform that is computationally efficient and ready to be transitioned on-board an aircraft.

## 2. EHSAs CONFIGURATION

The EHSAs used in this research is a typical electrohydraulic primary flight control actuator. It is composed of the hydraulic and the control parts. The first consists of one electrohydraulic servo-valve and a linear hydraulic actuator. The servo-valve is of the flapper-nozzle type and it is made up of two stages with the first stage receiving the current command as the input and using the torque motor in order to move the flapper thus creating a pressure drop at the ends of the second stage spool, which controls the flow to the hydraulic actuator. The control structure uses a position linear sensor as the feedback sensor for closed loop position control. The reference system for the EHSAs is shown in Figure 1. In order to ensure redundancy of the drives and, consequently, greater safety, two actuators acting on the same flight control surface are employed with the two EHSAs operating in an active-active, or active-standby mode.

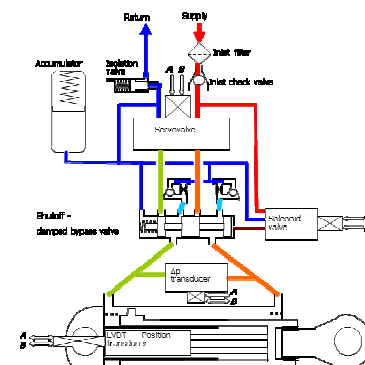


Figure 1. EHSAs reference system

## 2.1. EHSA signals

The typical structure of an EHSA for legacy aircraft allows for the acquisition of three kinds of information:

- Position command: corresponding to the position request processed by the flight control computer.
- Real position: information acquired by means of the LVDT and used to close the control position loop.
- Servo-valve current: generated by the controller coincident with the compensated error. It is used to control the valve.

## 2.2. Servo-valve degradation

The types of faults that most commonly occur in the EHSAs are well known, although no consolidated models for such failure modes exist which can be taken as a basis for predicting their fault progression. Although these fault growth models are not yet fully validated, their physical based approach ensures that the fault growth pattern is described correctly allowing for a virtual testing of the efficacy of health monitoring algorithms.

Possible degradation modes include:

- Reduction of the torque of the first stage torque motor. This can be the result of a shorting of adjacent coils of the torque motor due to the presence of metallic debris, or to a degradation of the magnetic properties of the materials. A progressively slower response of the servo-valve is obtained.
- Contamination of the first stage filter and nozzles. As dirt and debris accumulate in the first stage filter or in the nozzles, their hydraulic resistance increases which, in the end, leads to a slower response of the servo-valve.
- Stiffness variation of internal feedback spring, which is generally caused by yield in strength due to excessive loads or to normal aging of the component; involves hysteresis phenomena and instability.
- Increase of the backlash at the mechanical interface between the internal feedback spring and spool. This is the result of a wear due to the relative movement between these two parts giving rise to an increasing hysteresis in the servo-valve response, which leads to an instability.
- Variation of the friction force between spool and sleeve. This is due to a silting effect associated either with debris entrained by the hydraulic fluid or to the decay of the hydraulic fluid additives which tend to polymerize when the fluid is subjected to large shear stresses.
- Increase of the radial clearance between spool and sleeve and change of the shape of the corners of the

spool lands due to wear between these two moving parts.

In the absence of consolidated degradation models, progression of a degradation provisionally assumed to be a function of either usage time, or amplitude / frequency of commands, or both. In the study of the occlusion of the first stage filter it is considered to be a function of the square of flight hours.

## 3. PROGNOSTICS AND HEALTH MANAGEMENT

We introduce an integrated framework for fault diagnosis and failure prognosis that relies on systems engineering principles and takes advantage of physics of failure models, Bayesian estimation methods and measurements acquired through seeded fault testing and/or on-board the aircraft. The proposed Bayesian estimation framework for diagnosis and prognosis for nonlinear, non-Gaussian systems begins with a systems engineering process to identify critical components and their failure models, sensing and monitoring requirements and processing algorithms. Fundamental to this approach is the development of physics-based failure or fatigue models and the optimum selection and extraction of features or Condition Indicators (CI's) from raw data that form the characteristic signatures of specific fault modes. The latter are selected based on such criteria as sensitivity to particular fault modes and their correlation to ground truth data. The proposed framework employs a nonlinear state-space model of the plant, i.e. critical aircraft component, with unknown time-varying parameters and a Bayesian estimation algorithm called particle filtering to estimate the probability density function (PDF) of the state in real time (Orchard & Vachtsevanos, 2009). The state PDF is used to predict the evolution in time of the fault indicator, obtaining as a result the PDF of the RUL for the faulty component/system. A critical fault is detected and identified by calling on the particle filter-based module that expresses the fault growth dynamics. Prognosis has been called the Achilles' heel of CBM due to major challenges arising from the inherent uncertainty in prediction. Prognosis may be understood as the result of the procedure where long-term (multi-step) predictions - describing the evolution in time of a fault indicator - are generated with the purpose of estimating the RUL of a failing component. The same particle filtering framework and nonlinear state model suggested above will be used to estimate the RUL (Roemer, Byington, Kacprzynski, Vachtsevanos & Goebel, 2011)

Particle filtering has a direct application in the arena of fault detection and identification (FDI) as well as prediction of the time to failure of a critical component. Indeed, once the current state of the system is known, it is natural to implement FDI procedures by comparing the process behavior with patterns regarding normal or faulty operating conditions. (Vachtsevanos, Lewis, Romer, Hess & Wu,

2006; Arulampalam, Maskell, Gordon & Clapp, 2002). Similarly, particle filtering allows for the accurate prediction of the remaining useful life accounting robustly for uncertainty issues.

A fault diagnosis procedure involves the tasks of fault detection and identification (assessment of the severity of the fault). In this sense, the proposed particle-filter-based diagnosis framework aims to accomplish these tasks, under general assumptions of non-Gaussian noise structures and nonlinearities in process dynamic models, using a reduced particle population to represent the state pdf (Orchard, Kacprzyński, Goebel, Saha & Vachtsevanos, 2008). A compromise between model-based and data-driven techniques is accomplished by the use of a particle filter-based module built upon the nonlinear dynamic state model:

$$\begin{cases} x_d(t+1) = f_b(x_d(t), n(t)) \\ x_c(t+1) = f_t(x_d(t), x_c(t), \omega(t)) \\ f_p(t) = h_t(x_d(t), x_c(t), v(t)) \end{cases} \quad (1)$$

where  $f_b$ ,  $f_t$  and  $h_t$  are non-linear mappings,  $x_d(t)$  is a collection of Boolean states associated with the presence of a particular operating condition in the system (normal operation, fault condition)  $x_c(t)$  is a set of continuous-valued states that describe the evolution of the system given those operating conditions,  $f_p(t)$  is a feature measurement,  $\omega(t)$  and  $v(t)$  are non-Gaussian distributions that characterize the process and feature noise signals respectively. For simplicity,  $n(t)$  may be assumed to be zero-mean i.i.d. uniform white noise. At any given instant of time, this framework provides an estimate of the probability masses associated with each fault mode, as well as a pdf estimate for meaningful physical variables in the system. Once this information is available within the FDI module, it is conveniently processed to generate proper fault alarms and to inform about the statistical confidence of the detection routine. Furthermore, pdf estimates for the system continuous-valued states (computed at the moment of fault detection) may be used as initial conditions in failure prognostic routines, giving an excellent insight about the inherent uncertainty in the prediction problem. As a result, a swift transition between the two modules (FDI and prognosis) may be performed, and reliable prognosis can be achieved within a few cycles of operation after the fault is declared. This characteristic is, in fact, one of the main advantages of the proposed particle-filter-based diagnosis framework.

#### 4. PHM STRATEGY

One of the main difficulties for developing a prognostic system for EHSAs is the lack of knowledge regarding the loads acting on the wing surface and corresponding commands. An interesting solution, proposed from Jacazio,

Dalla Vedova, Maggiore, Sorli (2010), Mornacchi, Vignolo (2014) and Jacazio, Mornacchi, Sorli (2015), is to exploit the pre-flight time to carry out the prognostic analysis integrating this new procedure with the pre-flight checks.

This solution has two interesting advantages: the first is the possibility of stimulating the EHSAs with any kind of command, offering the possibility of developing commands that maximize the effect of degradation on the extracted features while the second is related to the loads acting on the wing surface. With the aircraft on the ground, the aerodynamic force depends only on atmospheric wind; therefore, it is small and does not affect the response of the servo actuator.

The strategy implemented in this work provides the stimulus, during the preflight operations, of the EHSAs with a ramp command with 33 mm/s ratio and a max amplitude equal to 50% of half-stroke of the actuator.

#### 4.1. Operational Scenario

The behavior of an actuator is strongly dependent on external conditions and the temperature of the hydraulic fluid. In order to simulate the EHSAs in conditions as close as possible to those encountered in flight, a possible operating scenario has been suggested. This includes a series of flights within the European network and, for every situation of pre-flight conditions identified, starting from real data, the oil temperature and the average velocity of the atmospheric wind are accounted. The data are shown in the graph of Figure 2.

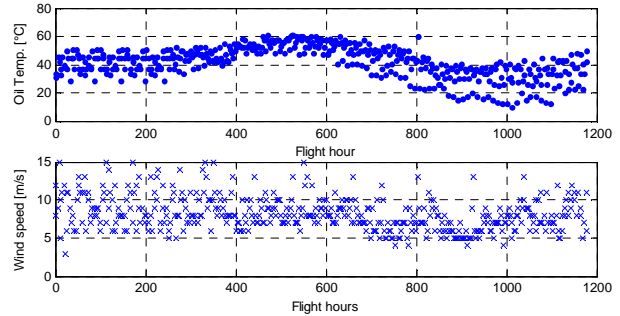


Figure 2. Example of oil temperature and wind speed

#### 5. FEATURE EXTRACTION

Feature or Condition Indicator (Cis) selection and extraction constitute the cornerstone for accurate and reliable fault diagnosis. The classical image recognition and signal-processing paradigm of data→information→knowledge becomes most relevant and takes central stage in the fault diagnosis case, particularly since such operations must be performed on-line in a real-time environment.

Fault diagnosis depends mainly on extracting a set of features from sensor data that can distinguish between fault classes of interest, detect and isolate a particular fault at its

early initiation stages. The remainder of this section evaluates a feature derived from the Hilbert transform to identify asymmetries because of turn-to-turn winding insulation faults.

A significant step in the development of robust and accurate PHM algorithms involves the extraction and selection of appropriate features or condition indicators from raw data. In our case, features are extracted using only the actuator position data and the servo-valve current. The analysis of the data obtained from the simulations has identified the first stage filter occlusion as a key indicator affecting two observable quantities.

Occlusion of the filter of the first stage of the servo valve leads to a lower response of the servo-command causing an increase of the time required for the actuator to reach the commanded position, as shown in

Figure 3, with a consequent growth of the error between the command and the real position. The increase of the error leads to enhancement of the servo-valve current generated by the controller (Figure 4). Until the current of servo-valve is below its saturation level, the controller can compensate for the growth of degradation thus limiting its effects on the system. After reaching the saturation threshold, the growth of the position error no longer results in an increase of the control current and, therefore, the system is no longer able to compensate for the growth of degradation.

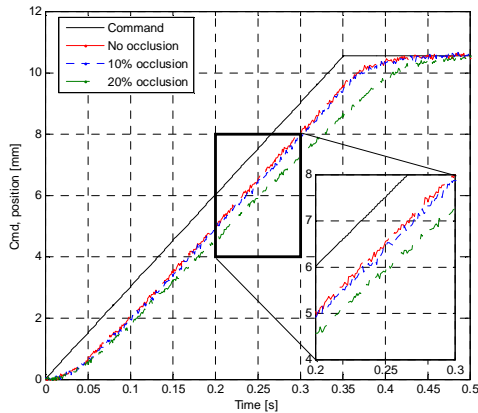


Figure 3. Influence of degradation on EHSA position

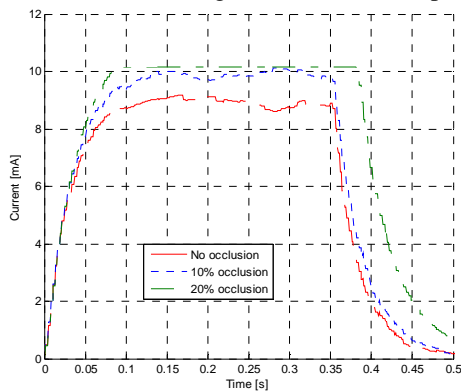


Figure 4. Influence of degradation on current

The data analysis has led to the definition of four different features that can be extracted by combining the acquired information. The features identified were then evaluated by appropriate metrics and one was selected and used in the prognostic algorithms. The features extracted from the data include:

- Mean error between real position and command; this is evaluated in the time range [0.15 0.35] s in order not to consider the initial and the end portion of the response. The feature is calculated as shown in following equation, where  $x_c$  is the command and  $x_r$  is the real position  

$$MeanError = mean(|x_c(t) - x_r(t)|)$$
- Mean speed, defined as the average speed of the actuator in the time range [0.15 0.35].
- The correlation coefficient between the position error and the current. In nominal conditions, there is a linear correlation between the current generated by the controller and the position error; this is due to the structure of the control logic, which provides a proportional part prevailing over the integral part. The presence of a degradation due to the saturation of the current and, consequently, to an increase of the error.
- Current fall time, defined as the time required for the current to return to a value less than 5% of its maximum value.

The values of the features functions of the occlusion of the servo-valve's first stage filter, as shown in Figure 5.

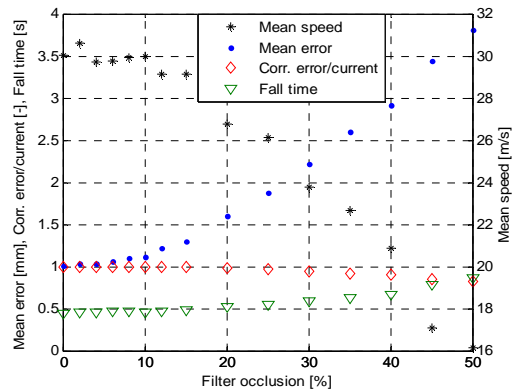


Figure 5. Features function of degradation

### 5.1. Feature performance

The features were evaluated by means of appropriate metrics, which lead to the definition and utility of those features that more accurately represent the state of the system. The metrics are:

- Accuracy measure: defined as the linear correlation between the occlusion of the first stage filter and the feature.

- Precision measure: the percent mean deviation of the feature with respect to the interpolation line used to describe the feature as a function of degradation:

$$PMD(x) = \frac{\sum |(x_i - \tilde{x}_i)/\tilde{x}_i|}{n} * 100$$

Where:  $x$  is the real value,  $\tilde{x}$  is the interpolated value and  $n$  is the sample number.

- Moving correlation: defined as the linear correlation between the degradation and the feature inside a moving window. The window size is 100 points with 99 points of overlap.

## 5.2. Feature selection

The choice of which feature should be used in prognostic algorithms was based on two main considerations: the metrics and previous (historical) knowledge. The metrics shown in Table 1 and Figure 6, exhibit an acceptable average error and are chosen for further processing.

At an operational level, the average error proves to be the best feature, since mean error is strictly related to the nature of the EHSAs. An increase of the average error between the actual position and the commanded one is easily linked to a degradation of the system. Other features like the current file time and mean rod speed are also physically linked to the behavior of the actuator but were not included in the targeted set.

Table 1: Features metrics

Feature	Correlation	PMD [%]
Mean error	0.979	1.356
Mean speed	-0.972	1.573
Corr. error/current	-0.945	1.759
Current fall time	0.949	1.245

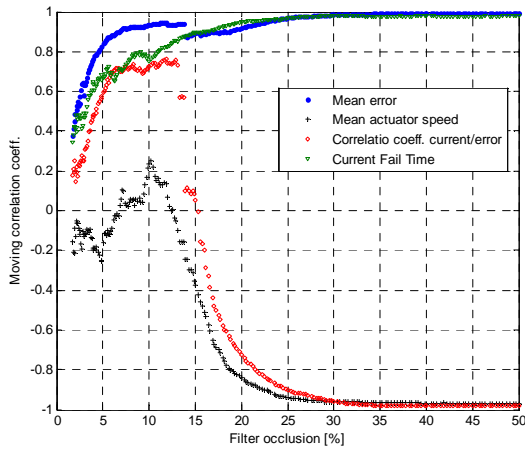


Figure 6. Moving correlation coefficient

## 6. ACTUATOR MATHEMATICAL MODEL

The mathematical model, implemented in Matlab-Simulink, is based on physical principles, and it is structured in different blocks following the composition of the EHSAs, allowing for rapid reconfiguration of the model when components have changed.

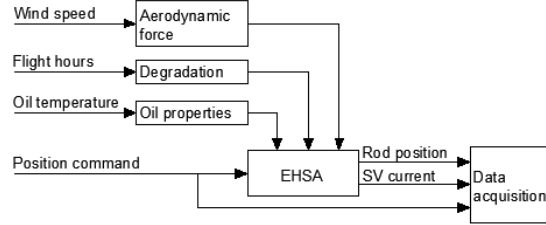


Figure 7. Scheme of mathematical model

The functional diagram of the model is shown in Figure 7, where inputs and outputs of the simulation model are highlighted with the latter coinciding with the signals available on the EHSAs. The EHSAs degradation that can be addressed by the virtual hardware include:

- EHSV feedback spring degradation (partial yielding, backlash increase)
- Increase of radial clearance between EHSV spool and sleeve
- EHSV spool friction increase
- Torque motor degradation
- Progressive clogging of an EHSV nozzle
- Contamination of the EHSV inlet filter
- Increase of the friction of the actuator spherical bearing
- Actuator seals damage
- Change of sensitivity of position sensor

The servo-valve torque motor is modelled using the Urata (2007a) magnetic circuit shown in Figure 8. Applying the proposed equations is possible to express the torque generated as a function of the magnetic flux density of each air-gap.

$$T = \frac{L_a A_g}{4\mu_a} \sum B_i^2 \quad (i = 1,2,3,4) \quad (2)$$

where  $B$  is the flux density in the air-gap,  $L_a$  is the distance between the left and right pole,  $A_g$  is the cross-sectional area of air-gap,  $\mu_a$  is the permeability of air.

The model also takes into account the influence of unequal air-gap thickness in servo valve torque motors, this is achieved by expressing the reluctance of the air-gap as function of air-gap thickness

$$R_i = \frac{l_0 \pm H \pm W \pm G \pm x_{arm}}{\mu_a A_g} \quad (i = 1,2,3,4) \quad (3)$$

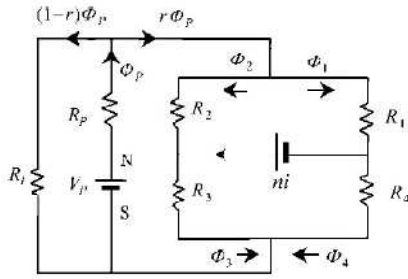


Figure 8. Magnetic torque motor circuit

In Eq. 3  $l_0$  is the nominal thickness and  $x_{arm}$  is the armature position and H,W,G are the coefficients that allow to express the misalignment of the armature, signs depend on the air-gap considered, for a more details see Urata (2007b).

The torque obtained from Eq. 2 combined with the dynamic equations of the flapper. The position of the flapper causes a variation of the flow from the two nozzles of hydraulic amplifier, and a consequent change in the pressure of the chambers placed at the ends of the spool. In the model the relationship between the position of the flapper and pressures at the ends of the spool is modeling diversity with the following equations

$$\begin{cases} P_A = G_{PA} * (x_f - G_{QA}x_s) \\ P_B = G_{PB} * (x_f - G_{QB}x_s) \end{cases} \quad (4)$$

where  $P_A$  and  $P_B$  are the pressures in the chambers,  $G_{PA}$  and  $G_{PB}$  are pressure gains and  $G_{QA}$  and  $G_{QB}$  are flow gains. Varying the value of the gains is possible to simulate contamination of the first stage filter or occlusion of one of the two nozzles.

The pressures determined by the equation (4) are used in the dynamic equation of the spool in order to estimate the opening of the flow ports. The equations that describe the kinematic system take into account the influence of the feedback spring force, coulomb and viscous friction and structural stiffness and damping. Furthermore, each parameter can be modified in order to simulate the degradation of the components.

The resulting servo-valve control flows, for each port, from the difference of the contributions from the supply and the return, the mathematical model calculates the individual contribution by exploiting the electrical similitude. Each port is represented as a circuit composed of two variable resistances placed in series  $R_C$  the laminar resistance and  $R_A$  the turbulence resistance.

$$\begin{cases} R_C = \frac{12\mu_{oil}(ol - x_s)}{2.5 * w_s h_s^3} & \text{for } ol \leq x_s \\ R_C = 0 & \text{for } ol > x_s \\ R_A = \frac{\rho_{oil} Q^2}{2C d^2 A^2} \end{cases} \quad (5)$$

where  $ol$  is the overlap,  $h_s$  is the spool radial gap and  $w_s$  is width of servo valve port.  $A$  is the area of the servo valve port.  $\rho_{oil}$  and  $\mu_{oil}$  are density and absolute viscosity, respectively.  $Q$  is the flow passing through the port and  $Cd$  is the discharge coefficient function of Reynold number and of the ratio between corner radius and port opening.

Using the value of the resistance, the model estimates the flow from each port with the equation (6)

$$Q = \frac{-R_C - \sqrt{R_C^2 - 4R_A * \Delta P}}{2R_A} * sgn(\Delta P) \quad (6)$$

where  $\Delta P$  is the pressure drop between the port.

A 3-DOF model describes the hydraulic linear actuator (Figure 9): the first two describe the rod, the surface position, and the last represents the deformation of the attachment point between the actuator and the fixed structure. The actuator coulomb friction is a function of the dynamic condition of the rod and of the geometrical and physical data of the seal as well as the pressures in the actuator chambers (Martini, L. J. 1984).

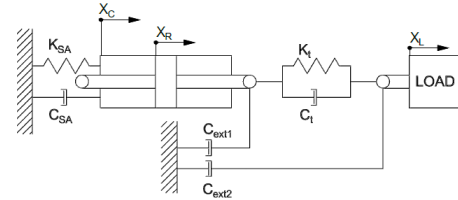


Figure 9. Actuator mathematical model

The mathematical model allows simulating the aerodynamic load acting on the wing surface, comprised of the sum of four components:

- Airplane velocity
- Atmospheric wind, obtained by a normally distributed random number
- A random number generator determines wind gust, whose amplitude and duration. Gusts occur in a random pattern.
- Turbulence, implemented using the Dryden model (Yeager, 2008).

Oil properties, such density, viscosity and bulk modulus, are computed using a set of equations that are functions of oil temperature.

A merit of the virtual hardware is a detailed physical representation of each EHSA component, enabling the rapid change of parameters and the evaluation of the corresponding changes of the EHSA performance, thus allowing the assessment of the effects of single and multiple degradations.

## 6.1. Validation

The model validation was carried out using data acquired through experimental testing and includes frequency responses of the EHSA and system responses to different stimuli. As shown by the example of Figure 10, the response of the mathematical model to a 2 Hz sinusoidal command, output of the model is very close to the actual behavior, concerning both the servo-valve and the actuator. The validation was carried out only for the hydraulic servo-system in nominal conditions.

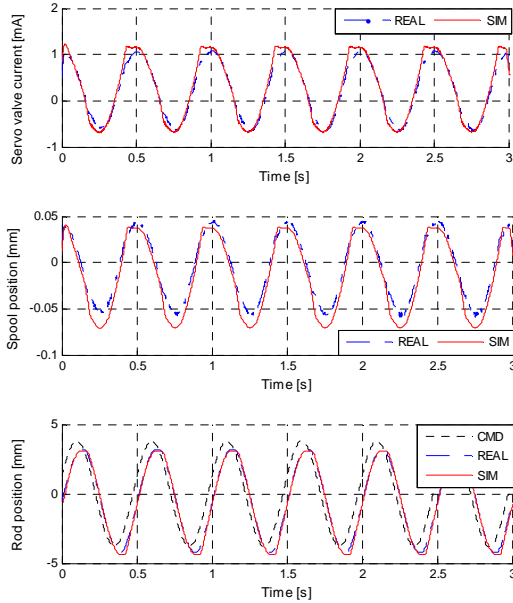


Figure 10. EHS mathematical model validation

## 7. DEGRADATION DETECTION

In the paper two different methodologies to detect the degradation; the first is a data-driven approach based on the data and the features extracted from the data while the second uses the particle filter in order to estimate the state of the system and identify the presence of degradation. In both approaches, the presence of the degradation is detected by comparing the curve of the feature in nominal conditions (baseline) with that obtained at the observation time.

### 7.1. Diagnostic performance requirement

Customer specifications are translated into acceptable margins for the *type I error* and *type II errors* in the detection routine:

- False alarm rate: defined as the probability of a false alarm. It coincides with *type I error* and equal to 5%
- Confidence: coincides with *100-Type II error [%]* and it expresses the level of confidence with which a degradation is detected. This work is set to 95%.

The algorithm itself will indicate when the confidence level, define as *100-Type II error [%]*, has increased to the desired level.

### 7.2. Data driven approach

The data-driven approach takes advantage of the data acquired during each stage of pre-flight. The histogram of the feature distribution that approximates the pdf curve is realized by using a moving window of 50 acquisitions with an overlap of 49. The baseline is achieved with 50 acquisitions made on the actuator in nominal conditions.

Figure 11 shows an example of degradation detection occurring after 698 flight hours and in the presence of an occlusion of 19% with an accuracy of 97%.

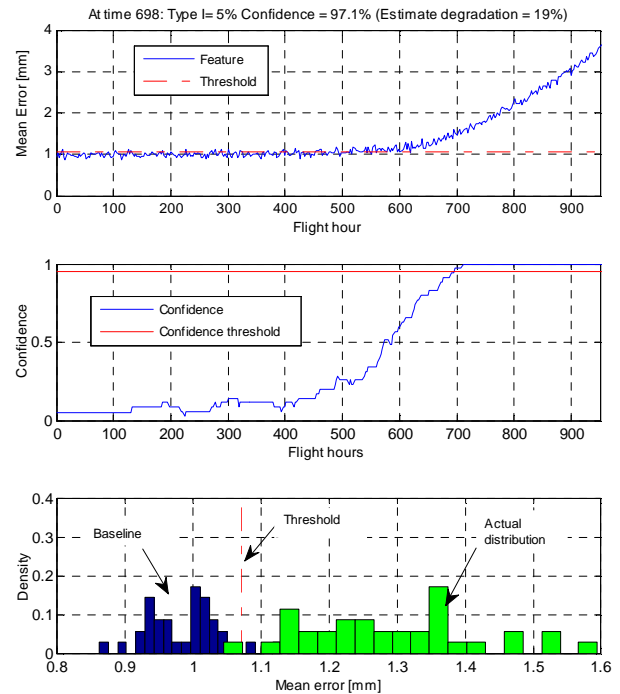


Figure 11. Detection data-driven

### 7.3. Particle filter approach

This approach exploits the particle filter framework to estimate the probability distribution of the extracted feature at each time instant for degradation detection purposes.

Applying the particle filter the system equations reduce to the form of Equation 7 allowing to estimate the occlusion of the first stage filter (coincident with continuous-valued states  $x_c$ ) and the pdf curve of the feature mean error.

$$\begin{cases} \begin{bmatrix} x_{d,1}(t+1) \\ x_{d,2}(t+1) \end{bmatrix} = f_b \left( \begin{bmatrix} x_{d,1}(t) \\ x_{d,2}(t) \end{bmatrix} + n(t) \right) \\ x_c(t+1) = x_c(t) + x_{d,2} dt (f_c(t+h) - f_c(t)) / h + \omega(t) \\ \text{Feature}(t) = h_t(x_c(t) + v(t)) \end{cases} \quad (7)$$

In equation 7:  $f_b$ ,  $f_c$  and  $h_t$  are non-linear mappings,  $x_{d,1}$  and  $x_{d,2}$  are Boolean states that indicate normal and faulty conditions, respectively,  $x_c(t)$  is a set of continuous-valued states that describe the evolution of the degradation those operating conditions,  $dt$  is the interval between  $t$  and  $t+1$ ,  $h$  is delta for numerical derivative and  $\omega(t)$  is noise describe like a normal distribution with zero mean.  $v(t)$   $v(t)$  is a normal distribution noise with mean equal to zero and sigma equal to the accuracy of the acquisition system, estimated as the sum of the position transducer error, position transducer demodulator error and A/D converter error. The initial conditions of the equation system (Eq. 7) are  $x_c=0$ ,  $x_{d,1}=1$  and  $x_{d,2}(0)=0$ .

The non-linear mappings  $f_c$  and  $h_t$  are functions that express the occlusion of the filter of the servo valve as a function of flight hours and the feature as a function of degradation, respectively. The equations are obtained using a symbolic regression tool, which starts with a set of data to identify the best fitting approximation. The selected functions for both cases offer the best compromise between accuracy of fitting and simplicity of the model, reducing the calculation time of the implemented algorithms.

The function  $f_c$  obtained using the symbolic regression is:

$$x_c(t) = a + b * t^2 + c * t^3 + d * t^4 \quad (8)$$

Where  $a, b, c, d$  are time-invariant coefficient and  $t$  is the flight hours. Figure 12 shows the comparison between the data and fitting curve, Table 2 shows the parameters related to the accuracy of the fitting.

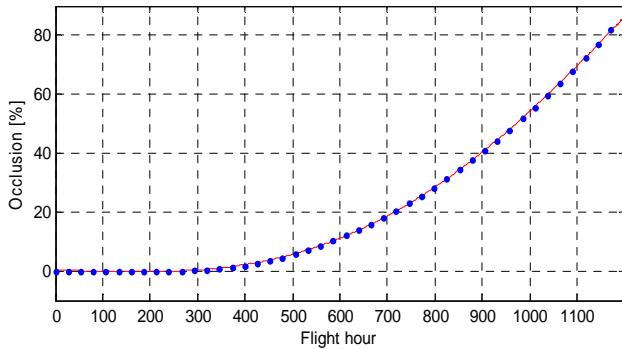


Figure 12. Occlusion model

Table 2: Occlusion model accuracy

R2	0.99993
Correlation coefficient	0.99996
Mean squared error	0.0436
Mean absolute error	0.1725

The function that represents  $h_t$ , expresses the feature as a function of the occlusion of the filter:

$$x_c(t) = e + f * x_c^2(t) + g * x_c^3(t) \quad (9)$$

Where  $e, f, g$  are time-invariant coefficient.

The results of symbolic regression are reported in Figure 3 and in Table 3 where the parameters related to the accuracy of the fitting are shown.

Table 3: Feature model accuracy

R2	0.99834
Correlation coefficient	0.99928
Mean squared error	0.0022
Mean absolute error	0.0319

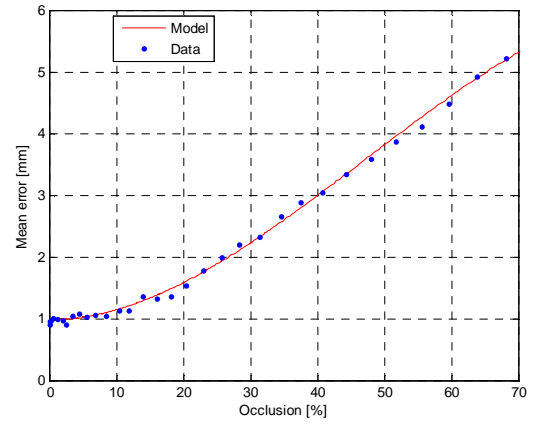


Figure 13. Feature model

The algorithm begins the detection process by defining the baseline, which is obtained by an estimate of the pdf of the features in the absence of degradation using the equation (7). The algorithm starts then from the initial condition of the filter estimate for each time instant and the new feature pdf curve is computed and compared with the baseline in order to identify the presence of degradation.

An example of identification of the degradation, shown in Figure 14, occurs after 680 flight hours and in the presence of an occlusion of 17% with an accuracy of 95.2%.

#### 7.4. Results

The detection algorithms were tested using ten simulated responses of the EHSA. The simulations were carried out by injecting diverse operational scenarios and different travel patterns within the European network; the EHSA behavior has been simulated with different environmental conditions and temperature profiles of the hydraulic fluid variables.

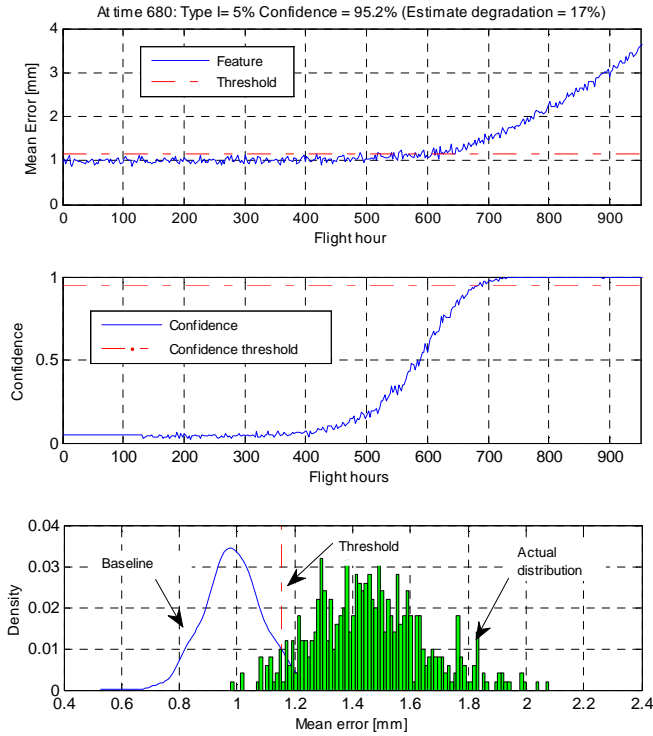


Figure 64. Detection particle filter

The average time to detection is 428 flight hours, which corresponds to an average occlusion equal to 19%.

The algorithm based on the particle filter exhibited better performance; it was able to identify the degradation in all conditions. Even the average time to detection is significantly lower; it is approximately 400 flight hours, coincident with about 16% of filter occlusion.

## 8. PROGNOSTICS

Prognosis is understood as the generation of long-term predictions describing the evolution in time of a particular signal of interest or fault indicator. In the work presented in this paper, predictions are based on an estimate of the evolution of the features' mean error. Its evolution is predicted using the particle filter presented previously, in particular the system of equations (7). The approach employs the previous state estimate to generate the a priori state pdf estimate for the next time instant.

We define by  $t_d$  the instant at which fault detection occurs, the particle filter then uses the pdf estimates for the system continuous-valued states  $x_c(t_d)$ , computed at the moment of fault detection, as initial conditions for the failure prognostic routines.

By using the state equation to represent the evolution of the fault dimension in time (Eq. 3), it is possible to generate a long-term prediction for the state pdf, in the absence of new

measurements, then use the predicted states  $x_c$  to estimate the resulting evolution of the feature.

The algorithm terminates the prediction when the estimated feature pdf for a given point in time completely surpasses the set threshold.

The limit, beyond which the component is considered failed, and thus needs to be replaced, has been estimated to be equal to a mean error of 4 mm.

Figure 15 shows example results of the RUL estimation; the end of life (EOL) of EHSA is 986 flight hours, which corresponds to a remaining useful life, defined as  $RUL = EOL - t_d$ , equal to 313 flight hours.

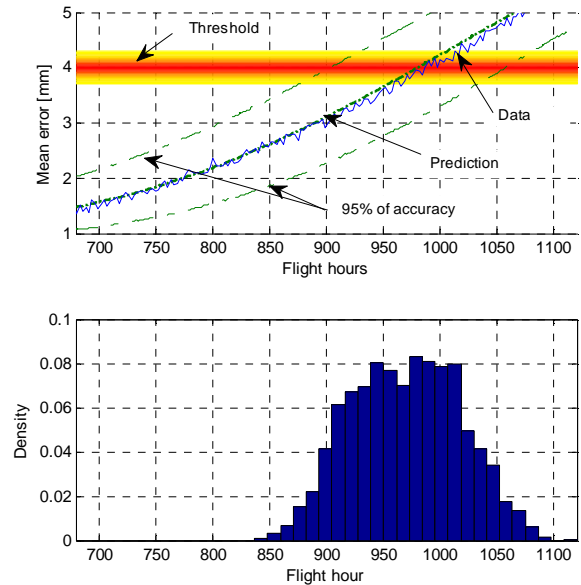


Figure 15. RUL prediction

### 8.1. Performance metrics

The performance of the prognostic algorithm was evaluated using the metrics proposed by Saxena, Celaya, Balaban, Gobel, Saha B, Saha S, and Schwabacher (2008). In particular, the following metrics were used:

- Prognostic horizon ( $H(i)$ ): defined as the difference between the current time index  $i$  and the end of prediction (EOP) utilizing data accumulated up to the index  $i$ , provided the prediction meets desired specification.

$$H(i) = EOP - i$$

- $\alpha$ - $\lambda$  performance: which allows to verify that the prediction to a generic  $\lambda$  instant has an accuracy  $\alpha$ .

$$(1 - \alpha) * r(t) \leq r_p(t) \leq (1 + \alpha) * r(t)$$

Where  $r_p$  is the predicted RUL at time  $t$ ,  $r$  is the real RUL,  $\alpha$  is the accuracy and  $t$  is defined as

$$t = P + \lambda(EOL - P)$$

Where  $P$  is the first prediction time instant and  $\lambda$  is window modifier.

- Relative Accuracy (RA): relative prediction accuracy at a specific time instance. Perfect score is RA=1.

$$RA(t) = 1 - \frac{|r(t) - r_p(t)|}{r(t)}$$

Where  $r_p$  is the predicted RUL at time  $t$ ,  $r$  is the real RUL and  $t$  is defined as

$$t = P + \lambda(EOL - P)$$

Where  $P$  is the first prediction time instant and  $\lambda$  is window modifier.

- Cumulative Relative Accuracy (CRA): normalized sum of the relative prediction accuracies. Perfect score is CRA=1.

$$CRA = \frac{1}{EOL - P + 1} \sum_{t=P}^{EOL} RA(t)$$

## 8.2. Results

The prognostic algorithm has shown good results with all ten data sets used; in all cases, the metrics demonstrated the robustness and accuracy of the algorithms. The mean prognostic horizon of the algorithm is equal to 292 flight hours. Example results for the metric  $\alpha$ - $\lambda$ , shown in Figure , demonstrate the accuracy of the algorithm in the estimation of the RUL, with the estimated value always within the limits of 20% for all data sets.

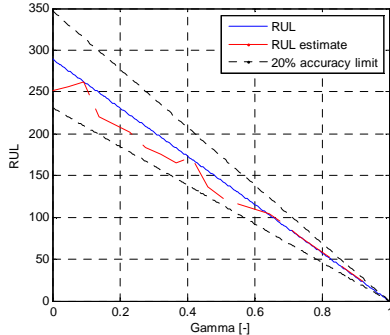


Figure 16.  $\alpha$ - $\lambda$  performance

Similarly, the RA and CRA metrics have demonstrated the accuracy of the algorithm in estimating the useful life; for all the data sets the 95% of the RA value is inside the range  $0.98 \div 0.88$ , the minimum value is equal to 0.85. Figure 17 exhibits the trend of the metric in the case of a single data set. The average value of CRA, for the ten data sets, is equal to 0.943. The best CRA is 0.948 while the worst is 0.941.

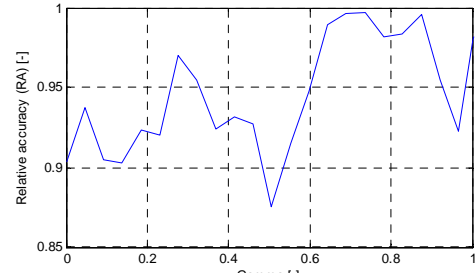


Figure17. Relative accuracy (RA)

## 9. CONCLUSIONS

This paper presented a particle-filter based fault detector capable of detecting the occurrence of a major fault mode in its incipient stages for a safety critical aircraft actuation system. Furthermore, the same basic estimation method was adopted for prediction of the remaining useful life of the actuator. An overview of a generic PHM architecture was presented and applied to a particular EHSA fault mode based on a FMECA study. The primary fault mode was modeled using physics-of-failure mechanisms indicating the primary failure effect. A feature was derived using statistical analysis to quantify the primary failure effect. Then, simulation data were acquired to validate the model. Although a specific system, an EHSA, was selected as the test-platform with a specific fault mode, the overall PHM architecture can be applied to an entire range of systems and application domains. In fact, similar techniques, which allow for early fault detection with acceptable performance in the presence of faults, are being developed for a wide variety of system actuators in both manned and unmanned air vehicles. Therefore, the concept of using system health information (diagnosis and prognosis) is at the forefront of modern space and avionics applications requiring increasingly sophisticated diagnostic and prognostic systems that are robust, reliable, and relatively inexpensive.

## ACKNOWLEDGEMENT

This work was supported by Lufthansa Technik AG; we appreciate their contribution to the development and validation of the mathematical model by providing to the research team actuators and technology applied to test benches.

## REFERENCES

- Arulampalam, M. S., Maskell, S., Gordon, N., & Clapp, T. (2002). A tutorial on particle filters for online nonlinear/non-Gaussian Bayesian tracking. *IEEE Trans. Signal Process*, vol. 50, no 2, pp.174–188
- Brown, D., Georgoulas, G., Bae, H., Vachtsevanos, G., Chen, R., Ho, Y.H., Tannenbaum, G., & Schroeder, J.B. (2009a). Particle filter based anomaly detection for aircraft actuator systems. *Aerospace conference, 2009 IEEE* , pp.1-13, March 7<sup>th</sup>-14<sup>th</sup>.

- Brown, D., Georgoulas, G., Bole, B., Pei, H. L., Orchard, M., Tang, L., Saha, B., Saxena, A., Goebel, K., & Vachtsevanos, G. (2009b). Prognostics Enhanced Reconfigurable Control of Electro-Mechanical Actuators. *Annual conference of the Prognostics and Health Management Society PHM09*, San Diego, USA, September 27<sup>th</sup> – October 1<sup>st</sup>.
- Byington, C.S., Watson, M., & Edwards, D. (2004). Data-driven neural network methodology to remaining life predictions for aircraft actuator components. *2004 IEEE Aerospace Conference, Proceedings*, vol. 6, pp.3581-3589, March 6<sup>th</sup> – 13<sup>th</sup>
- International Air Transport Association (IATA) (2011). Airline Maintenance Cost Executive Commentary - An exclusive benchmark analysis (FY2009 data) by IATA's Maintenance Cost Task Force
- Jacazio, G. (2008). The Evolution of Fly-by-Wire Flight Control Systems. *Guest speaker presentation at the IASTED conference on Modelling, Identification, and Control*, Innsbruck, Austria, February 11<sup>th</sup> - 13<sup>th</sup>
- Jacazio, G., Maggiore, P., Della Vedova, M. & Sorli, M. (2010). Identification of Precursors of Servovalves Failures for Implementation of an Effective Prognostics. *Proceedings of the 4th International Conference on Recent Advances in Aerospace Actuation Systems and Components*, Toulouse, France, May 5<sup>th</sup> – 7<sup>th</sup>.
- Jacazio, G., Mornacchi, A., & Sorli, M. (2015). Development of a prognostics and health management system for electrohydraulic servoactuators of primary flight controls. *5<sup>th</sup> International Workshop on Aircraft System Technologies AST2015*, Hamburg, Germany, February 24<sup>th</sup> – 25<sup>th</sup>.
- Marla, L., Vaaben, B., Barnhart, C. (2011) Integrated disruption management and flight planning to trade off delays and fuel burn; Report 16.2011 - DTU Management Engineering; December 2011
- Martini, L. J. (1984), Reciprocating Seals - Pistons and Cylinders. In CRC Press, *Practical Seal Design* (pp. 108-131). New York
- Mornacchi, A., & Vignolo, M. (2014). Health Management System for the Hydraulic Servoactuators of Fly-by-Wire Primary Flight Control Systems. *European Conference of Prognostics and Health Management Society PHME14*, Nantes, France, July 8<sup>th</sup> – 14<sup>th</sup>.
- Narasimhan, S., Roychoudhury, I., Balaman, E., & Saxena, A. (2010). Combining Model-Based and Feature-Driven Diagnosis Approaches – A Case Study on Electromechanical Actuators. *21st International Workshop on the Principles of Diagnosis (DX-10)*, Portland, USA, October 13<sup>th</sup> - 16<sup>th</sup>.
- Orchard, M., Kacprzynski, G., Goebel, K., Saha, B., & Vachtsevanos, G. (2008). Advances in Uncertainty Representation and Management for Particle Filtering Applied to Prognostics. *Annual Conference of the Prognostics and Health Management Society PHM08*, Denver, USA, October 6<sup>th</sup> – 9<sup>th</sup>.
- Orchard, M., & Vachtsevanos, G. (2009). A Particle Filtering Approach for On-Line Fault Diagnosis and Failure Prognosis. *Transactions of the Institute of Measurement and Control*, vol. 31, no. 3-4, pp. 221-246.
- Pohl, T., (2013). Cost per hour of downtime per aircraft is ~ 10,000 USD+ more, in *SAP for Aerospace & Defense*
- Roemer, M., Byington, C., Kacprzynski, G., Vachtsevanos, G., & Goebel, K. (2011). Prognostics, in *Systems Health Management with Aerospace Applications*. Wiley, pp. 281-295
- Saxena, A., Celaya, J., Balaban, E., Goebel, K., Saha, B., Saha, S., & Schwabacher, M. (2008). Metrics for evaluating performance of prognostic techniques. *International Conference on Prognostics and Health Management*, pp.1,17, October 6<sup>th</sup> - 9<sup>th</sup>
- Urata, E. (2007a). On the torque generated in a servo valve torque motor using permanent magnets. *Proceedings of the Institution of Mechanical Engineers, Part C: Journal of Mechanical Engineering Science*. vol. 221 (Issue 5), pp. 519-525
- Urata, E. (2007b). Influence of unequal air-gap thickness in servo valve torque motors. *Proceedings of the Institution of Mechanical Engineers, Part C: Journal of Mechanical Engineering Science*. vol. 221 (Issue 11), pp. 1287-1297
- Vachtsevanos, G., Lewis, F., Roemer, M., Hess, A. & Wu, B. (2006). Intelligent Fault Diagnosis and Prognosis for Engineering Systems. John Wiley & Sons, Inc.
- Yeager, J. (1998). Implementation and Testing of Turbulence Models for the F18-HARV Simulation. *NASA CR-1998-206937, Lockheed Martin Engineering & Sciences*.

## BIOGRAPHIES

**Mornacchi A.** is a mechanical engineer and a PhD student in mechanical engineering. His primary interest is in the areas of prognostic for aerospace servosystems and modelling and simulation of hydraulic and electromechanical servos. He is a member of the servosystems and mechatronics group of the Department of Mechanical and Aerospace Engineering.

**Jacazio G.** is professor of applied mechanics and of mechanical control systems. His main research activity is in the area of aerospace control and actuation systems and of prognostics and health management. He is a member of the SAE A-6 Committee on Aerospace Actuation Control and Fluid Power Systems, and a member of editorial board of the international society of prognostics and health management.